

# Attosecond Control of Ionization Dynamics

P. Johnsson,<sup>1,\*</sup> J. Mauritsson,<sup>1,2</sup> T. Remetter,<sup>1</sup> A. L'Huillier,<sup>1</sup> and K. J. Schafer<sup>2</sup>

<sup>1</sup>*Department of Physics, Lund University, P. O. Box 118, SE-221 00 Lund, Sweden*

<sup>2</sup>*Department of Physics and Astronomy, Louisiana State University, Baton Rouge, Louisiana 70803-4001, USA*

(Dated: February 8, 2022)

Attosecond pulses [1, 2] can be used to initiate and control electron dynamics on a sub-femtosecond time scale. The first step in this process occurs when an atom absorbs an ultraviolet photon leading to the formation of an attosecond electron wave packet (EWP). Until now, attosecond pulses have been used to create free EWPs in the continuum, where they quickly disperse [3, 4, 5, 6, 7]. In this paper we use a train of attosecond pulses, synchronized to an infrared (IR) laser field, to create a series of EWPs that are below the ionization threshold in helium. We show that the ionization probability then becomes a function of the delay between the IR and attosecond fields. Calculations that reproduce the experimental results demonstrate that this ionization control results from interference between transiently bound EWPs created by different pulses in the train. In this way, we are able to observe, for the first time, wave packet interference in a strongly driven atomic system.

The modulation of photon absorption by wave packet interference (WPI) has been used in molecular systems as a probe of nuclear dynamics on a femtosecond time scale [8], and in Rydberg atoms as a probe of electron dynamics on a picosecond time scale [9]. WPI is a sensitive tool for probing quantum dynamics because it depends on the spatial and temporal behavior of the wave packet in the confining potential. This is most easily appreciated by considering two well separated excitation pulses that create two initially localized wave packets in a manifold of excited states. The total excitation probability will be the simple sum of the integrated population in each wave packet *unless* some part of the first wave packet returns to the region of space where it was created during the time when the second wave packet is created, enabling the two to interfere.

In this Letter we present attosecond WPI experiments using a train of ultraviolet (UV) attosecond pulses to ionize either helium or argon atoms in the presence of an IR field. The attosecond pulses are phase locked to the IR field since their spacing in time is precisely one half of the laser period. The central energy of the pulses,  $\approx 23$  eV, is higher than the ionization energy of argon (15.8 eV), but below that of helium (24.6 eV), as shown in Fig. 1a. We demonstrate the ability to control the ion yield in helium through the delay between the two fields, an effect which is absent in argon. We attribute this ionization control to interference between transiently bound EWPs created in helium which can modulate the probability that an electron is excited out of the atomic ground state. Calculations based on integration of the time-dependent Schrödinger equation (TDSE) show that the contrast in the ionization probability versus the IR-UV delay is an order or magnitude larger than what is achieved with a single pulse, and that the contrast grows as the number of pulses in the train is increased. Both

of these effects are hallmarks of WPI, seen here in the attosecond domain and for a strongly driven system.

Details of the experiment can be found in the Methods section. The spectral and temporal characteristics of the attosecond pulse train (APT) used to excite the atoms are presented in Fig. 1a, while examples of momentum distributions obtained from UV ionization alone are shown in Fig. 1b and 1c for helium and argon, respectively. The IR laser field, a replica of the laser pulse used to generate the UV pulses, was recombined with the APT after a variable delay line and focused into the detection chamber with an intensity of  $1.3 \times 10^{13} \text{ W}\cdot\text{cm}^{-2}$ . A crucial point is that this laser intensity is too low to excite any population out of the ground state by itself. This means that the ground state is connected to the excited bound and continuum states only when an attosecond pulse is present, an essential condition for observing WPI. Also of importance is the fact that although the IR laser field is weak from the point of view of an electron in the ground state, it is strong from the point of view of an electron excited out of the ground state. At peak amplitude, the IR field suppresses the Coulomb potential by  $\sim 7$  eV at the saddle point, which is enough to unbind all of the single excited bound states of helium. Furthermore, this barrier suppression changes very slowly with intensity, scaling as  $I^{1/4}$ . Our method therefore results in creating attosecond EWPs in a strong oscillating laser field.

Figure 2 shows our main experimental result, the delay dependence of the ion yields,  $P_{\text{ion}}$ , from helium and argon. For  $\text{Ar}^+$  (red squares), there is no measurable effect of the IR field while for  $\text{He}^+$  (blue circles) the ion yield is increased by a factor of four when the IR field is present. In addition, the  $\text{He}^+$  yield exhibits a modulation as a function of the UV-IR delay. The depth of the modulation is  $\approx 35\%$  and the period is equal to half the laser period. This modulation is the signature of WPI of attosecond EWPs in our experiment.

To gain insight into the results presented in Fig. 2, we have performed calculations based on the integration of

---

\*Electronic address: per@eng-johnsson.se

the TDSE [10, 11], as explained in more detail in the Methods section. The ion yields obtained at the end of the interaction are indicated in Fig. 2 as solid red and solid blue lines for argon and helium respectively, showing good agreement with the experiment. In addition, the calculations show that without an IR field, the ionization probability in He is equal to the excitation probability, meaning that no population is left in the excited bound states. As indicated in Fig. 1a, the spectrum of the UV pulses overlaps poorly with the accessible excited bound states of helium, and the atom is limited to absorbing photons belonging to the 17th harmonic, leading to immediate ionization.

In Fig. 3a, we show more complete theoretical results for He. Shown are both the probability that an electron is excited out of the ground state ( $P_{\text{exc}}$ , blue line) and the ionization probability ( $P_{\text{ion}}$ , red line). The difference between these probabilities is the probability to remain in an excited state after the IR pulse ends ( $P_{\text{bnd}}$ , green line). Two features are immediately apparent. First, the modulation in the  $\text{He}^+$  yield is caused by the fact that the amount of population excited out of the ground state by the APT in the presence of the IR field is modulated as a function of UV-IR delay. Second, the ionization of the population promoted out of the ground state by the APT is incomplete, leaving 30-40% of the promoted population in excited states after the IR field is over.

The delay dependence of the  $\text{He}^+$  yield has two contributions. First, each pulse in the APT excites population in the presence of an IR field that distorts the atomic potential by an amount that depends on the IR-UV delay. A single attosecond pulse would therefore probe solely the atom's ability to absorb light near the ionization threshold in the presence of an electric field which can be as high as  $\sim 10^8$  V/cm. Our calculations show that the modulation in the ion yield due to such a single attosecond pulse is about 1-3% over the intensity range covered by the experiment, 10 times smaller than the observed effect. The other contribution to the delay dependence is from WPI. This temporal interference in the total excitation probability comes about if an EWP created by one pulse in the train has some probability to be near the ion core when a later packet is being excited by a different pulse in the train. This requires that an EWP excited by a single pulse takes more than one half cycle to completely ionize. Indeed, at all delays we find that the EWP excited by a single attosecond pulse takes one to several IR cycles to completely ionize, fulfilling this condition for WPI.

WPI also causes the excitation probability to scale non-linearly with the number of pulses in the train. In the absence of WPI the relative modulation in the total excitation probability versus delay is the same for different length pulse trains. In Fig. 3b, we plot the normalized excitation probability for APTs of different length, changing from a single pulse (the 1 fs envelope) to two or more. We see that the relative modulation increases as the APT length is increased. We also note that the

delay curve reverses its shape when the number of pulses is increased from one to two or more. In argon, by contrast, the total excitation is linear in the length of the pulse train.

By its nature, WPI is a very sensitive probe of the electron dynamics in a bound system. In our system these dynamics are most easily altered by changing the IR intensity. In Fig. 3c we plot the magnitude of the calculated relative modulation (*i.e.* the contrast) versus peak IR intensity for intensities ranging from 0.1 to  $3.0 \times 10^{13}$  W·cm $^{-2}$  and a 10 fs APT (blue line). As can be seen, the contrast is a very sensitive function of the field amplitude. For comparison, the contrast from using a single 370 as pulse is shown (red line). In this same range of intensities the amount of population ionized after the IR pulse is over ranges from 40-100% of the total population excited out of the ground state, and exhibits a very complicated dependence on the IR intensity.

Additional support for the WPI picture that we present can be found in the experimental measurements of the energy-resolved angular distributions from helium and argon, presented in Fig. 4. For argon (Fig. 4a) the IR field only redistributes the energy of the ionized electrons, depending on the phase of the IR field at the time they enter the continuum. The highest energy electrons are created when the attosecond pulses are timed so that ionization takes place at the zero-crossings of the electric field ( $\omega\tau = n\pi$ ), when the momentum transfer from the field to the electronic wave packet is maximum [5, 6]. The momentum distributions from argon (Fig. 4b and 4c) show the difference between the two delays that results in the greatest and least number of high energy electrons. The angular distributions remain rather broad for all delays. In contrast to this, the photoelectron momentum distributions from helium (Fig. 4e and 4f) are strongly peaked along the polarization axis of the IR field, reflecting the fact that most of the ionization occurs via electrons that escape over the suppressed Coulomb barrier along the polarization direction. In addition, at the experimental IR intensity the highest energy electrons are observed when  $\omega\tau \approx 0.3\pi + n\pi$ , which corresponds neither to the maxima or zeros of the IR electric field, as seen in Fig. 4d. This illustrates the complex wave packet dynamics discussed previously, which leads to different ratios between bound and free populations as well as between numbers of low and high energy electrons depending on the UV-IR delay and the IR intensity.

The WPI that we have observed has a number of similarities and a few important differences as compared to “traditional” WPI. In more conventional WPI, the motion takes place on a purely bound potential surface and the WPI is controlled by changing the delay between pulses. In our case, the delay between attosecond pulses is fixed at one half the IR cycle, but the amplitude and phase of the IR field at which the EWPs are created is easily changed. Also, the EWPs are only transiently bound and so both the total population and the energy-resolved angular distributions can be measured as a func-

tion of the various parameters in the experiment and compared to theory. WPI offers a unique tool to study the behavior of electrons in a strongly driven atom or molecule, since the EWPs are created in the center of the potential well at a well-controlled time.

A number of modifications to the experiments we have presented here are accessible in the near future. For instance, the wavelength of the laser field can be varied, perhaps all the way to the mid-infrared, which would allow the time difference between the attosecond pulses to be varied. Most importantly perhaps, it should be possible to study the WPI as a function of the APT duration as was done in the theoretical calculations. This could be done in a polarization gating scheme by varying the gate duration [12].

In conclusion, we have demonstrated that excitation/ionization dynamics can be controlled using an APT in combination with an IR field. Previous attosecond experiments have used the UV pulse to control the time at which an ionization process takes place [3, 4, 5, 6, 7, 13]. The control demonstrated in this experiment is, to the best of our knowledge, the first use of an attosecond pulse to modulate the probability of an ionization event. When coupled to angular-resolved photoelectron distributions it opens the way for future study of the detailed dynamics of ultra broadband EWPs in driven atomic and molecular systems.

## Methods

### *Experiment*

The APT was synthesized from high-order harmonics generated in xenon by focusing 35 fs, 796 nm (1.56 eV photon energy) pulses from a 1 kHz Ti:sapphire laser to an intensity of  $\approx 8 \times 10^{13} \text{ W}\cdot\text{cm}^{-2}$  in a 3 mm long windowless gas cell filled to a static pressure of  $\approx 20$  mbar. The APT was filtered spatially by passing it through a 1.5 mm diameter aperture, and spectrally using a 200 nm thick aluminium filter. The spatial filter removes contributions to the harmonic emission from the longer quantum paths, while the aluminium filter blocks the remaining IR and the intense low-order harmonics [14]. The spectrum of the APT is shown in Fig. 1a and consists of harmonics 11 to 17, with a central energy of 23 eV. The pulses were characterised using the RABITT technique (reconstruction of attosecond beating by interference of two-photon transitions) [1, 15], and the average duration of the bursts was found to be 370 as with the temporal profile shown in the inset in Fig. 1a.

The dressing IR pulse, a delayed replica of the pulse generating the harmonics, was collinearly overlapped with the APT before both beams were refocused into the spectrometer by a toroidal platinum mirror. Recombination was achieved using a mirror with a hole in the centre, through which the APT was sent, and on which the dressing pulse was reflected. The delay of the dress-

ing pulse relative to the APT was finely controlled by a mirror mounted on a piezo-electric translation stage. To obtain a good estimate of the IR intensity, calibration was performed by measuring  $\text{Xe}^+$  and  $\text{Xe}^{2+}$  ion yields as a function of intensity. In addition, these estimates were confirmed by comparison with the observed ponderomotive shift [16] in the photoelectron spectra. The absolute timing between the APT and the IR field was not accessible experimentally, and has been chosen to fit the results of the TDSE calculations.

A velocity map imaging spectrometer was used for detection, having the advantage of being able to operate either in electron imaging [17] or in ion time-of-flight mode. For both ion and electron detection, the target gas was injected by means of an atomic beam pulsed at 50 Hz. The ion yield measurements were carried out in time-of-flight mode, the signal being collected with a boxcar integrator using active background subtraction based on the laser shots arriving with no target gas present. The 2D projections of the momentum distributions of the photoelectrons were recorded by means of an MCP-assembly and a CCD-camera, and from these the 3D momentum distributions were obtained using the iterative inversion procedure described in [18].

### *Theory*

For the TDSE calculations we use the single active electron (SAE) approximation, in which we assume that only one electron interacts with the field, while the others remain in the ground state. This approximation has been extensively tested for both alkali metal and rare gas atoms and found to produce results which compare well with experiments [19, 20]. The atomic potentials used in the SAE calculations were the standard Hartree-Fock potential for helium, and a pseudo-potential in argon [21]. These potentials reproduce the single electron excited states very well. To simulate the experiments we use an IR pulse whose electric field envelope is a cosine function with a FWHM in intensity of 35 fs, and an APT whose electric field envelope is a somewhat sharper  $\cos^2$  function with a FWHM in intensity of 10 fs. The total population excited is calculated as one minus the population remaining in the ground state at the end of the pulse, while the total ionization is calculated either from the photoelectron spectrum [22] or by running the calculation for 10 additional IR cycles and calculating the probability to remain in the vicinity of the ion. A variety of other field envelopes (*e.g.* APTs with varying numbers of pulses and a constant IR pulse envelope) were used to check details of our analysis.

## Acknowledgments

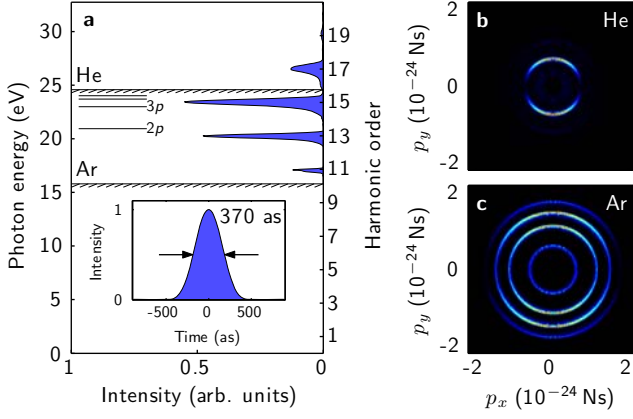
We are grateful to S. Thorin, Dr. F. Lépine and Prof. M. J. J. Vrakking for help with the imaging spectrometer.

This research was supported by the Marie Curie Research Training Network (MRTNCT-2003-505138, XTRA), the Crafoord Foundation, the Knut and Alice Wallenberg Foundation, the Swedish Research Council and the National Science Foundation through Grant No. PHY-0701372.

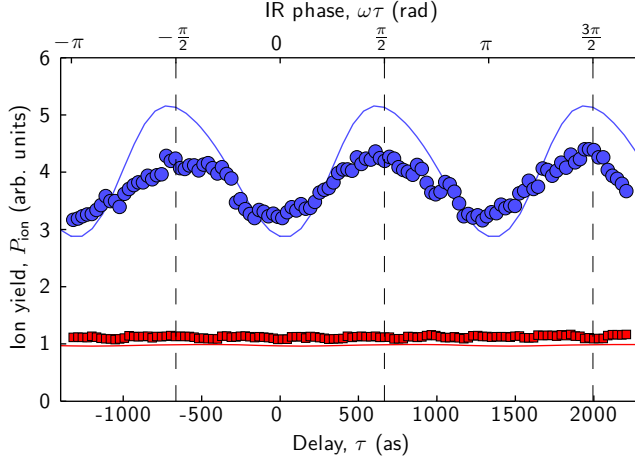
### Competing financial interests

The authors declare that they have no competing financial interests.

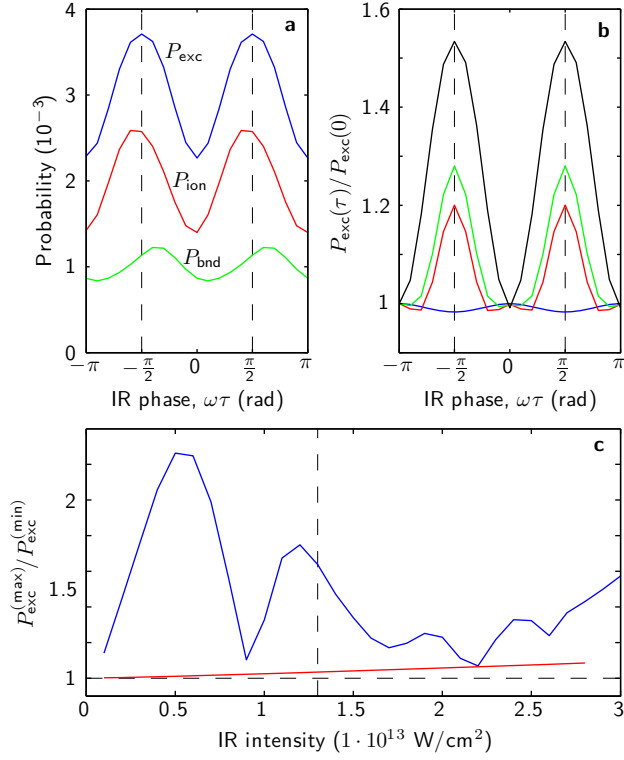
- 
- [1] Paul, P. M. *et al.* Observation of a Train of Attosecond Pulses from High Harmonic Generation. *Science* **292**, 1689 (2001).
  - [2] Drescher, M. *et al.* X-Ray Pulses Approaching the Attosecond Frontier. *Science* **291**, 1923 (2001).
  - [3] Kienberger, R. *et al.* Steering Attosecond Electron Wave Packets with Light. *Science* **297**, 1144 (2002).
  - [4] Kienberger, R. *et al.* Atomic transient recorder. *Nature* **427**, 817 (2004).
  - [5] Goulielmakis, E. *et al.* Direct Measurement of Light Waves. *Science* **305**, 1267 (2004).
  - [6] Johnsson, P. *et al.* Attosecond Electron Wave Packet Dynamics in Strong Laser Fields. *Phys. Rev. Lett.* **95**, 013001 (2005).
  - [7] Remetter, T. *et al.* Attosecond Electron Wave Packet Interferometry. *Nature Phys.* **2**, 323 (2006).
  - [8] Scherer, N. F. *et al.* Fluorescence-detected wave packet interferometry: Time resolved molecular spectroscopy with sequences of femtosecond phase-locked pulses. *J. Chem. Phys.* **95**, 1487 (1991).
  - [9] Noordam, L. D., Duncan, D. I. & Gallagher, T. F. Ramsey fringes in atomic Rydberg wave packets. *Phys. Rev. A* **45**, 4734 (1992).
  - [10] Kulander, K. C., Schafer, K. J. & Krause, J. L. Time-Dependent Studies of Multiphoton Processes. In *Atoms in Intense Laser Fields* (Academic Press, San Diego, 1992).
  - [11] Krause, J. L., Schafer, K. J. & Kulander, K. C. High-order harmonic generation from atoms and ions in the high intensity regime. *Phys. Rev. Lett.* **68**, 3535 (1992).
  - [12] Sola, I. J. *et al.* Controlling attosecond electron dynamics by phase-stabilized polarization gating. *Nature Phys.* **2**, 319 (2006).
  - [13] Drescher, M. *et al.* Time-resolved atomic inner-shell spectroscopy. *Nature* **419**, 803 (2002).
  - [14] López-Martens, R. *et al.* Amplitude and Phase Control of Attosecond Light Pulses. *Phys. Rev. Lett.* **94**, 033001 (2005).
  - [15] Muller, H. G. Reconstruction of attosecond harmonic beating by interference of two-photon transitions. *Appl. Phys. B* **74**, 17 (2002).
  - [16] Bucksbaum, P. H., Freeman, R. R., Bashkansky, M. & McIlrath, T. J. Role of the ponderomotive potential in above-threshold ionization. *J. Opt. Soc. Am. B* **4**, 760 (1987).
  - [17] Eppink, A. T. J. B. & Parker, D. H. Velocity map imaging of ions and electrons using electrostatic lenses: Application in photoelectron and photofragment ion imaging of molecular oxygen. *Rev. Sci. Instrum.* **68**, 3477 (1997).
  - [18] Vrakking, M. J. J. An iterative procedure for the inversion of two-dimensional ion/photoelectron imaging experiments. *Rev. Sci. Instr.* **72**, 4084 (2001).
  - [19] Walker, B. Precision Measurement of Strong Field Double Ionization of Helium. *Phys. Rev. Lett.* **73**, 1227 (1994).
  - [20] Gaarde, M. B. *et al.* Strong species dependence of high order photoelectron production in alkali metal atoms. *Phys. Rev. Lett.* **84**, 2822–2825 (2000).
  - [21] Kulander, K. & Rescigno, T. Effective potentials for time-dependent calculations of multiphoton processes in atoms. *Computer Physics Communications* **63**, 523 (1991).
  - [22] Schafer, K. J. & Kulander, K. C. The energy analysis of time-dependent wave functions: Application to above threshold ionization. *Phys. Rev. A* **42**, 5794 (1990).

**Figure 1, Johnsson et al.**

**FIG. 1: Experimental pulses and single-photon momentum distributions.** **a**, Spectrum of the UV pulses used in the experiment shown in relation to the ionization potentials of helium and argon. For helium, some of the excited states have been indicated for comparison. The corresponding temporal profile is a train of pulses spaced by half the IR laser cycle. The inset shows the temporal profile of the attosecond pulses in the train, each with a duration of 370 as, as reconstructed from the RABITT measurements. Panels **b** and **c** show experimental photoelectron momentum distributions from single-photon ionization by the APT in helium and argon, respectively, with the polarization of the light parallel to the  $p_y$ -axis. **b**, In helium, only a single ring corresponding to ionization by harmonic 17 can be seen, since this is the only spectral component having sufficient energy to overcome the ionization potential. The angular distribution is peaked along the polarization axis, as expected for single-photon ionization from an  $s$ -state. **c**, In argon, the full bandwidth of the APT contributes to the ionization and four rings corresponding to harmonics 11 to 17 can be seen. Since the ionization starts from a  $p$ -state, the resulting angular distribution is a superposition of  $s$ - and  $d$ -states, with contributions also along the  $p_x$ -axis.

**Figure 2, Johnsson et al.**

**FIG. 2: Control of the ion yield.** Experimentally measured ion yields,  $P_{\text{ion}}$ , for  $\text{He}^+$  (blue circles) and  $\text{Ar}^+$  (red squares) as a function of the delay  $\tau$  between the attosecond pulses and the IR field, at an intensity of  $1.3 \times 10^{13} \text{ W}\cdot\text{cm}^{-2}$ . We use a sine convention for the IR electric field so that delays,  $\tau$ , which are multiples of  $\pi/\omega = 1330 \text{ as}$ , where  $\omega$  is the IR laser frequency ( $\hbar\omega = 1.56 \text{ eV}$ ), correspond to the attosecond pulses overlapping the zero-crossings of the IR field. All yields are normalised to those obtained with only the APT present. In helium a clear modulation is observed which is not seen in argon. Also shown in the figure are the calculated ion yields at an IR intensity of  $1.3 \times 10^{13} \text{ W}\cdot\text{cm}^{-2}$  for  $\text{He}^+$  (blue solid line) and  $\text{Ar}^+$  (red solid line). These were obtained using UV and IR fields that closely match the experimental parameters: the APT has a 10 fs FWHM (full width at half maximum in intensity) duration and the IR pulse is 35 fs FWHM, and agree well with the experimental results.

**Figure 3, Johnsson et al.**

**FIG. 3: Detailed theoretical study of ionization in helium.** **a**, Calculated probabilities for removal of an electron from the ground state ( $P_{\text{exc}}$ , blue line), ionization ( $P_{\text{ion}}$ , red line) and remaining in an excited bound state ( $P_{\text{bnd}}$ , green line) as a function of the phase of the IR field at the time of the attosecond pulses, for an APT with a FWHM of 10 fs and a 35 fs IR field with a peak intensity of  $1.3 \times 10^{13} \text{ W}\cdot\text{cm}^{-2}$ . **b**, Excitation probability,  $P_{\text{exc}}$ , versus delay for different APTs, normalized to the excitation probability for zero delay in each case. The FWHM of the APT intensity envelope is 1 fs (blue line), 2 fs (red line), 4 fs (green line) or 8 fs (black line). The 1 fs envelope corresponds to an isolated attosecond pulse. **c**, Contrast in  $P_{\text{exc}}$  (defined as the maximum excitation probability divided by the minimum) for various peak intensities of the IR field (blue line). The APT has a FWHM of 10 fs. For comparison, the contrast obtained with a single attosecond pulse is also shown (red line).

Figure 4, Johnsson et al.

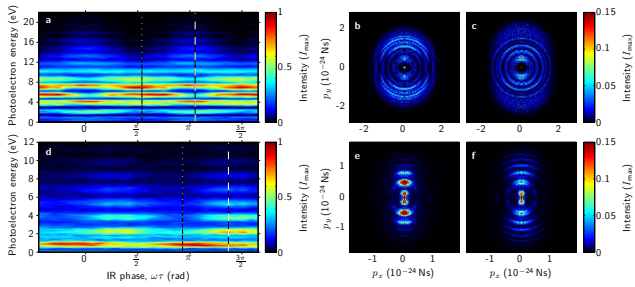


**FIG. 4: Experimental photoelectron spectra and momentum distributions.** Photoelectron spectra as a function of the delay between the attosecond pulses and the IR field from argon (**a**) and helium (**d**). **b** and **c**, Momentum distributions obtained at the delays corresponding to the dotted and dashed lines in **a**. **e** and **f**, Momentum distributions obtained at the delays corresponding to the dotted and dashed lines in **d**. The polarization directions of the UV and IR fields are parallel to the  $p_y$ -axis.